Supporting Information for

Single Lévy states – Disorder Induced Energy Funnels in Molecular Aggregates

*Aboma Merdasa[†], Ángel J. Jiménez[‡], Rafael Camacho[†], Matthias Meyer[†], Frank Würthner[‡], Ivan G. Scheblykin[†,]**

Table of Content Page

SI-I. Absorption and fluorescence of PBI-1 monomers and J-aggregates

PBI-1 dyes aggregate when dissolved in methylcycolhexane (MCH) and remain in monomeric form when dissolved in dichloromethane (DCM). Figure SI-1 shows the bathochromic shift of the absorption by 1950 cm^{-1} upon aggregation. The width of the J-aggregates absorption spectrum is smaller than that of the monomer absorption due to motional narrowing. Indicated in the figure are also the widths of the monomer (max at 570 nm) and J-aggregate (max at 660 nm) fluorescence bands.

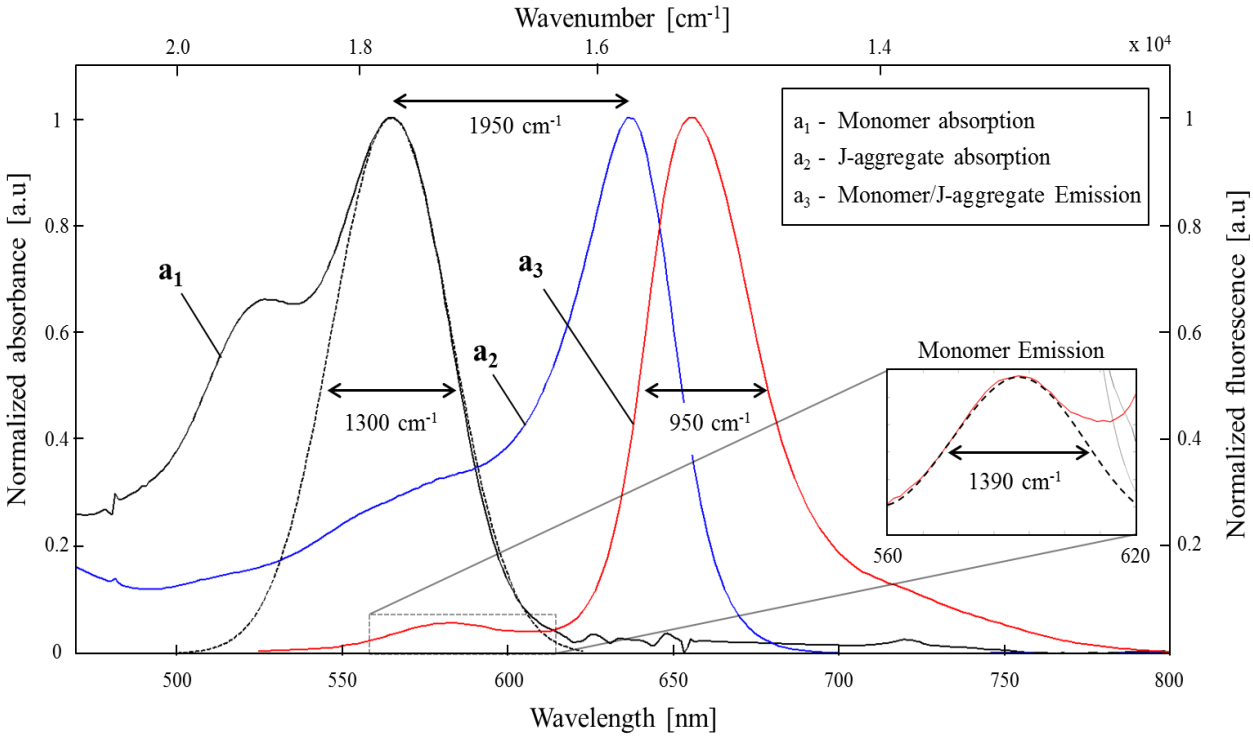

Figure SI-1 | Absorption and fluorescence of PBI-1 monomers and aggregates in solution.

Estimations of the monomer absorption and fluorescence band widths were made using a Gaussian fit. The monomer absorption contains an extra vibronic peak at 520 nm, however we only took into account the 0-0 band in the estimation of the width. The monomer emission can be seen together with the aggregate emission since not all PBI-1 dyes were aggregated at the given conditions.

SI-II. Single Aggregate Analysis

This section provides further detail on the analysis applied to the spectra of all aggregates. The main objective of this analysis was to use statistical methods to find aggregates of interest (showing spectral fluctuations) in order to create an unbiased platform for selecting aggregates for further analysis.

Singular Value Decomposition (SVD)

For the analysis of single aggregate spectra we applied a statistical method called *singular value decomposition*. In general, SVD is a method used when studying large data sets where *m* variables are observed *n* times creating a matrix of *m* x *n* elements. SVD is an extremely powerful method applied in a diverse number of fields. Detailed description of the general method can be found in literature.[1] Here, we aim to describe how we used it with the fluorescence spectral data set.

We apply SVD to a single aggregate spectral data (intensity at m=163 wavelengths (number of pixels per spectrum) measured over n=500 frames) to see if the data can be represented as linear combinations of only a few key spectral features, whose intensities vary independently over time. Using SVD, these key spectral features are given in the form of spectral basis vectors (eigenvectors), which are orthogonal to one another and create a new coordinate system. The principle behind SVD is that the new coordinate system is chosen in such a way that the first spectral basis vector represents the most important spectral feature of the data set. The second spectral basis vector accounts as much as possible for the spectral features that cannot be described by the first spectral basis vector, and so on.

Mathematically, each spectral feature is represented by an eigenvector of length *m*. Each eigenvector has a *singular value* that describes how important this spectral feature is for the whole data set. The first eigenvector has the highest *singular value,* representing the most relevant spectral feature. The second eigenvector accounts for additional fluctuations that cannot be described by the first eigenvector. Thus, the second *singular value* is smaller than the first. By this logic, each additional eigenvector will have a lower *singular value*. By analyzing the relative magnitudes of the singular values, we can determine how many different key spectral features are present in a single aggregate spectral data set.

Figure SI-2a shows all experimental spectra of aggregate #78. Figure SI-2b shows the *singular values* of the spectral basis vectors (eigenvectors). We see that the first two spectral basis vectors have *singular values* that are nearly 2 orders of magnitude larger than the rest. This indicates that they alone account for the majority of the spectral features in the entire data set. This becomes easier to understand from Figure SI-2c where the first two spectral basis vectors are plotted. From the figure we see that a linear combination of the first two spectral basis vectors is enough to describe all the spectra in Figure SI-2a quite well.

Analyzing the relative magnitudes of the singular values allows us to obtain the so-called ‘noise floor’ (red dashed line in Figure SI-2b). From the noise floor we can quantify the signal-to-noise ratio (SNR) of the *singular values*. When analyzing each individual aggregate spectral data, any *singular value* having an SNR of 2 or lower were considered irrelevant. Out of the 217 aggregates, 15 were found to have more than one significant spectral feature and these are plotted in Figure 2a of the paper.

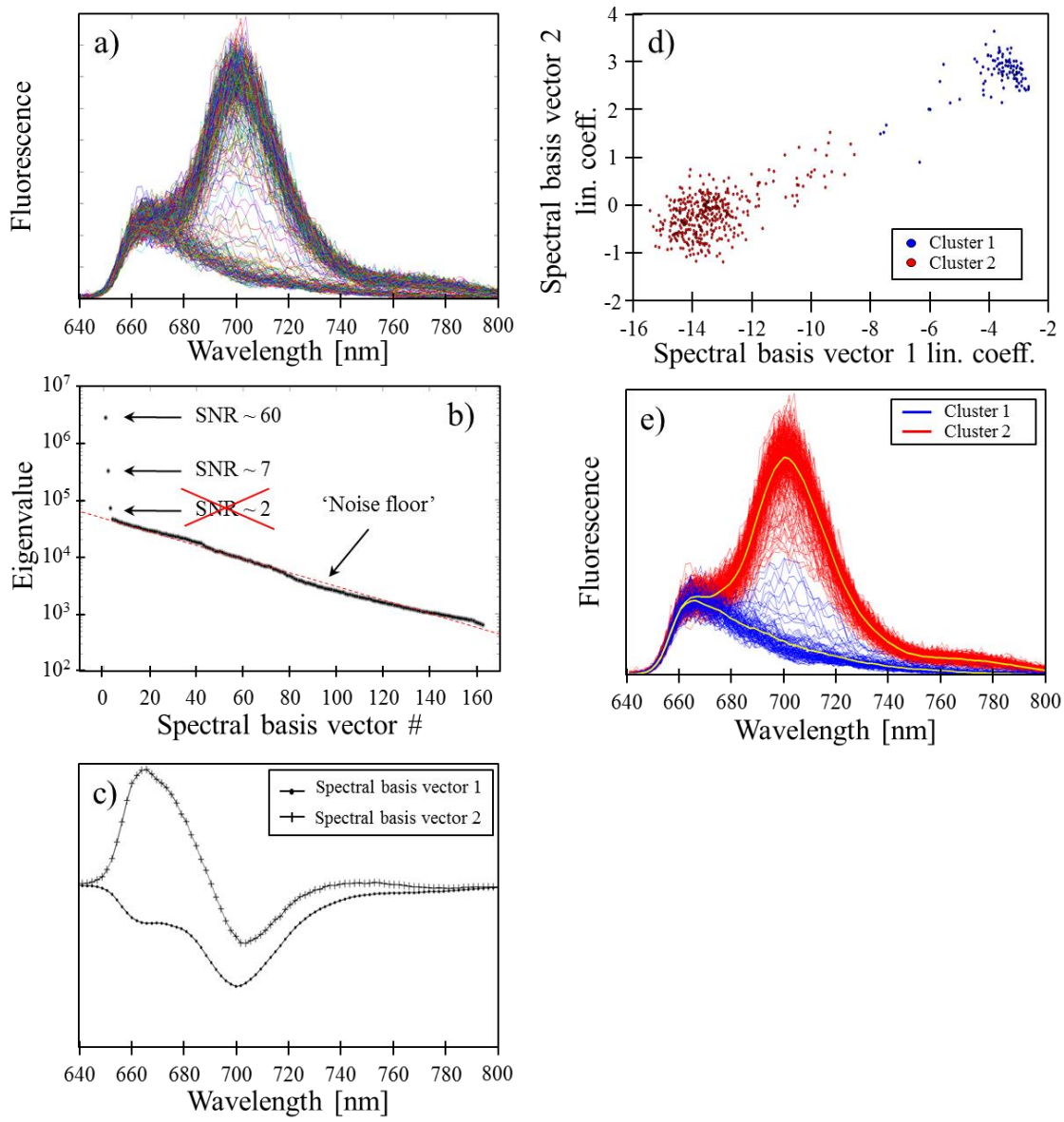

Figure SI-2 | Spectral analysis procedure applied to aggregate #78

(a) shows the original data for aggregate #78 where all spectra are plotted from all frames. (b) shows the singular values for each spectral basis vector. The noise floor is indicated with a red dotted line and the SNR for the 3 first singular values are also shown where the 3rdsingular value is considered irrelevant (crossed out in red). (c) shows the first two spectral basis vectors. (d) plots the projection of the whole data set to the plane defined by the two spectral basis vectors plotted in (c). Using the Hierarchical Clustering method we are able to separate each frame into two clusters indicated with the different colors. Plotting the spectra of all frames belonging to each cluster in their respective color we see in (e) that spectra belonging to each cluster are similar. The mean spectrum of each cluster is plotted in yellow.

Hierarchical Clustering

After analyzing all aggregates we found that those exhibiting spectral fluctuations had predominantly two spectral basis vectors describing most of the fluctuations. This means that every spectrum in each frame can be described by linear combination the first two spectral basis vectors.

Plotting the linear coefficients belonging to the first two spectral basis vectors as points in a plane(one point for each spectra, Fig. SI-2(d)), we could apply a technique called Hierarchical Clustering.[2]The method calculates the Euclidean distance between all data points and separates them into a user-defined number of clusters. Since the number of relevant *singular values* indicates how many different key spectral features exist in the data set, it makes sense to try to divide the data points into the equal amount of clusters. After applying the Hierarchical Clustering method to the 500 data points (frames) we see there are two distinct clusters (colored in blue and red). All frames of each cluster therefore exhibit similar spectral features. This allowed us to not only see the different spectral features and which frames they were in, but also correlate any other fluorescence behavior (blinking, localization of emission) to these spectral features. In Figure SI-2e we plot the spectra belonging to each cluster with the same color coordination (cluster 1 – blue, cluster 2 – red). We also plot the mean spectrum of each cluster in yellow.

Double-band Fitting

To further analyze all spectra we look at the mean spectra of each cluster (plotted with yellow lines in Figure SI-2e). For simplicity we will refer to the mean spectra of cluster 1 and 2 as the 'blue' and 'red' spectra respectively. It appears as if the red spectrum is a combination of the blue spectrum and an additional peak. To separate these we first analyzed the blue spectrum using a mixed Gaussian-Lorentzian fit (Eqs. SI-1and SI-2),

$$G(\lambda) = \frac{I_p}{\{1 + [4M\xi^2]/\Gamma^2\} exp\{(1 - M)[4ln2\ \xi^2]/\Gamma^2\}} \tag{SI-1}$$

$$\xi = \frac{(\lambda - \lambda_p)}{\left(1 + \alpha_{GL}(\lambda - \lambda_p)\right)/\Gamma} \tag{SI-2}$$

where λ_p - peak wavelength, I_p - intensity at the band peak, M - degree of mixing between the Gaussian and Lorentzian shape (0 = pure Gaussian, 1 = pure Lorentzian), Γ - a common width for both shapes, and α_{GL} is the asymmetry constant ($-2 \leq \alpha_{GL} \leq 2$).[3] The use of a mixed Gaussian-Lorentzian profile is a first approximation when applied to an asymmetric line shape subject to

homogeneous broadening effects. Equations SI-1 and SI-2 use a common width for both profiles and which has been denoted with Γ not to be confused with other places where a width is discussed in the text.

We applied the fit to all the spectra belonging to cluster 1 and found that, besides intensity fluctuations, the spectral shapes were rather stable with parameters for the peak wavelength at λ_p = 665 nm, common width Γ = 25 nm and asymmetry constant α_{GL} = 0.8.

When fitting the spectra in cluster 2, 10 parameters were used for two peaks where 5 were fixed for the blue spectrum according to the values obtained above. This allowed us to subtract the blue spectrum from red spectrum to plot them independently (now referring to them as the blue and red emission bands).

Figure SI-3 shows an example of the band-separation in two frames where (a) the blue band is present and (b) where both bands are present. The original spectrum in each frame is plotted in black, and the blue and red bands are plotted in blue and red respectively.

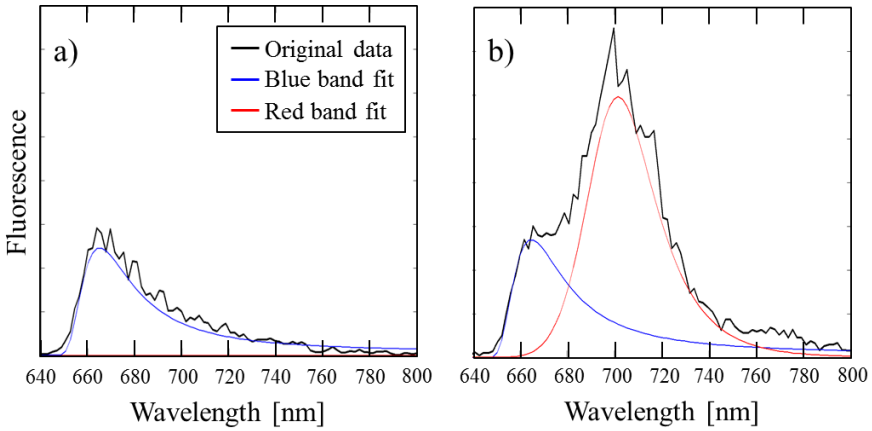

Figure SI-3 | Example of band separation through double peak fitting

Comparison of two frames where the red band is absent (a - frame 1) and where it is present (b – frame 200) for aggregate #78.

Figure SI-4 shows an example of the peak separation of aggregate #139 applied in all frames.(a) shows the full spectra and (b-c) show the separated blue and red bands after applying the band-separation procedure.

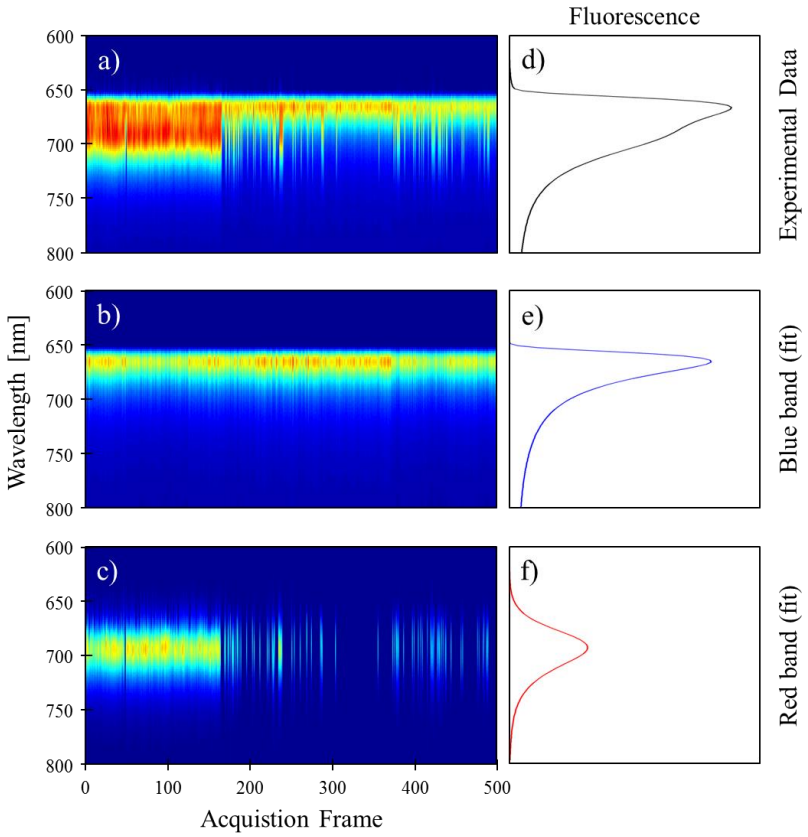

Figure SI-4 | Example of spectral band-separation

Fluorescence band separation of aggregate #139 in time. (a) shows the experimental data without any fitting applied to it. After using Eq. SI-1 and 2 we can separate every spectrum into two parts where the blue band is shown in (b) and the red band in (c). The z-scale is the same in all figures (a-c). (d-f) shows the integrated spectra over all acquisition frames where the intensity scale is the same for all plots.

Separating the bands and integrating the intensity of each allowed us to see the intensity contribution of each band to the total fluorescence. In the following section, the peak separation procedure is applied to all frames of the 15 selected aggregates.

SI-III. Statistics Analysis of Multiple Aggregates

In this section we aim to show that the fluctuationsseen in aggregate #78 are not unique to that aggregate, but similar fluctuations are seen in other aggregates too.

In order to find aggregates exhibiting potentially interesting behavior, we used the procedure outlined in section SI-II (comparison of the *singular values*) which yielded 15 out of 217 aggregates having an additional red-shifted band in at least one acquisition frame (plotted in paper, Figure 2a).

The double-band fitting procedure was applied to all spectra which could not be exclusively fitted with the blue spectrum only. The intensity contribution of each band was measured as a fraction of the total intensity. Figure SI-5shows a histogram of the intensity contribution of the

red band to the total fluorescence from roughly 4300 analyzed frames out of 6900 (15 aggregates having either 500 or 200 acquisition frames).

We can conclude that when the red band was present, it was responsible for appoximately one half of the fluorescence.

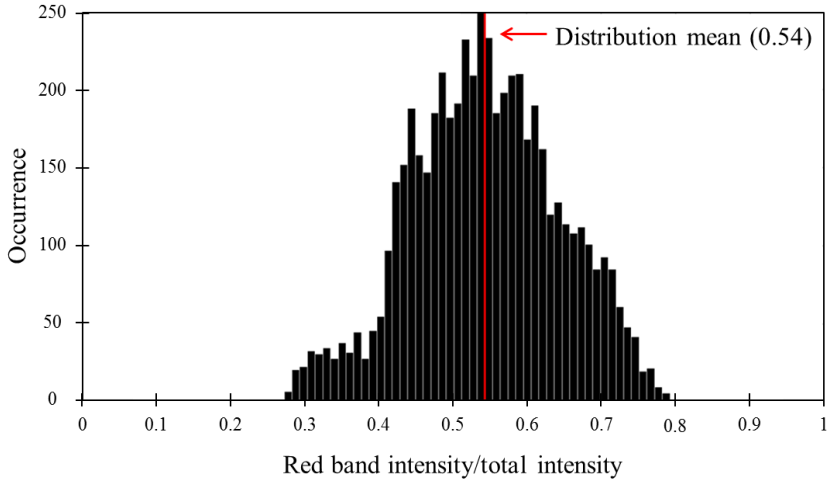

Figure SI-5 | Contribution of the Red band to the total fluorescence intensity.
Relative contribution of the red band to the total fluorescence in each acquired frame for the 15 selected aggregates from the SVD procedure (see SI-II).

SI-IV. Analyzed Aggregate 'Movies'

Below is a description of 5 selected aggregate ‘movies‘ showing the behavior of their fluorescence in intensity, spectral and spatial domains. Table SI-1 summarizes how well the fluctuations are visible in each domain. Each domain recieves a grade between 1-5 (not visible-well visible) depending on how clearly a red-shifted band, distinct intensity levels, or well-defined localization clusters are seen. Each movie has also a short summarizing comment.

Aggregate Movie name	Spectral Domain	Intensity Domain	Spatial Domain	Comment
SI-M_{63}	4	5	4	The aggregate exhibits a clear correlation between all domains. Intensity blinking due to the ‘on/off‘ switching of the red band is very strong. Red emission is also very localized compared to the blue.
SI-M_{78}	5	5	4	This aggregate (#78) shows a clear correlation in all domains. It is the example discussed in the main text of the article.
SI-M_{128}	5	5	3	Interesting behavior since it appears that we are dealing with 3 states. The original ‘blue‘ and ‘red‘ bands are observed throughout the entire acquisition while there is an additional band centered around 680 nm that switches ’on‘ and ‘off‘. Could be an indication of the presence of

				more than one Lévy state.
SI-M_{139}	4	4	5	The aggregate shows a very clear correlation in all frames. However, the spectrum does not show an obvious separation between the red and blue bands, (see also Figure SI-4) but with the correlation to the spatial domain, the behavior becomes more clear. The spatial domain shows exceptional clustering. As Figure SI-4 shows, band separation of this aggregate spectra revealed two bands.
SI-M_{173}	3	3	5	The spectral fluctuations seem to be dominated by the band centered at 680 nm. The switching of this band correlates very well with the spatial fluctuations, however, the intensity levels are not stable. This could have something to do with the exposure time being too long to resolve the fast blinking behavior of this aggregate.

Table SI-1 | Summary of the additional single aggregate movies

SI-V. 2D Polarization Imaging of *Single-Aggregate* Sample

In 2D-POLIM the fluorescence intensity *I* of the sample (an isolated aggregate) is measured for a set of combinations of the excitation and emission polarization angles, φ_{ex} and φ_{em}, respectively.[4] From this data we construct a 2D function that receives the name of polarization portrait, $I(\varphi_{ex}, \varphi_{em})$, for each isolated aggregate. In essence, the polarization portrait contains the correlation between the sample's emission polarization and the electric field's direction of the linearly polarized excitation light.

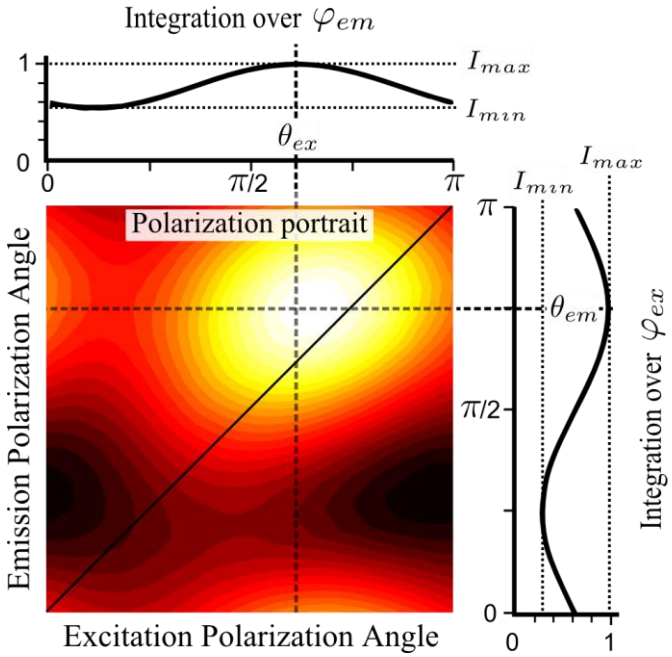

Figure SI-6 | Polarization portrait and calculation of parameters

Integration of the polarization portrait (Figure SI-6) over the excitation (φ_{ex}) or emission (φ_{em}) polarization angle yields a one dimensional function having the following functional form:

$$I(\varphi_{em}) = \int_0^{\pi} I(\varphi_{ex}, \varphi_{em})\, d\varphi_{ex} = \bar{I} + M_{em} \cos\big(2(\varphi_{em} - \theta_{em})\big) \tag{SI-3}$$

$$I(\varphi_{ex}) = \int_0^{\pi} I(\varphi_{ex}, \varphi_{em})\, d\varphi_{em} = \bar{I} + M_{ex} \cos\big(2(\varphi_{ex} - \theta_{ex})\big) \tag{SI-4}$$

where, M_{em} is the modulation depth in emission (excitation - M_{ex}), θ_{em} is the emission polarization phase (excitation – θ_{ex}), and $\bar{I}$ is the average value of the corresponding 1D function.

Further, the modulation depths can be calculated from the maximum (I_{max}) and minimum (I_{min}) values (Figure SI-6) of the corresponding 1D function:

$$M = \frac{I_{max} - I_{min}}{I_{max} + I_{min}} \tag{SI-5}$$

Correlation between modulation depth in excitation and emission

Figure SI-7shows histograms of (a) the modulation depth in excitation - M_{ex} (also referred to as fluorescence detected linear dichroism) and (b) modulation depth in emission - M_{em} (emission polarization degree), as well as the correlation between the two (c) for 223 individual aggregates from a *single-aggregate* sample. The data points are shifted up from the diagonal, which is an indication of energy transfer towards less randomly polarized emitting sites.[4] A broad distribution of M_{ex} indicates that aggregates are not straight rods, but rather possess worm-like shapes.

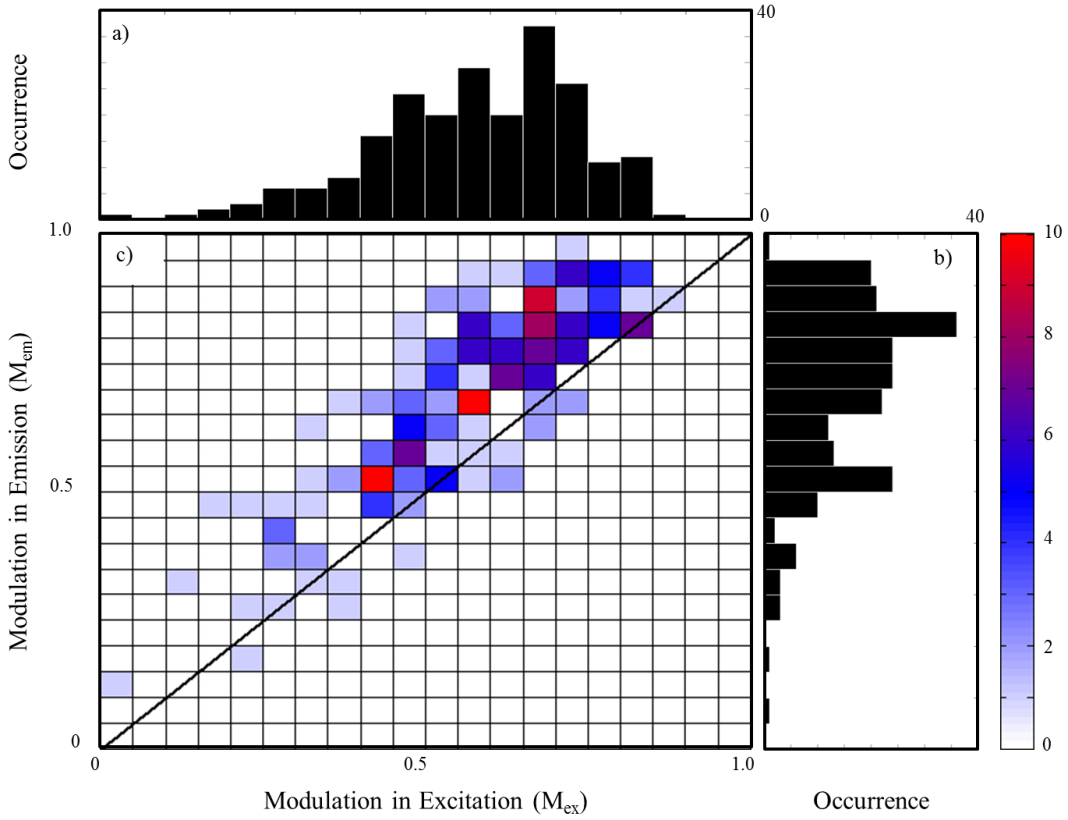

Figure SI-7 | Modulation Depth in Excitation vs. Modulation Depth in Emission for individual aggregates.

SI-VI. Simulation of the exciton band

Frenkel Exciton Hamiltonian with Disorder

J-aggregate exciton states and optical transitions are described using the Frenkel exciton Hamiltonian of a disordered 1-D chain[5] in the nearest-neighbor approximation according to;

$$H = \sum_{n=1}^{N} E_n \, |n\rangle\langle n| \; + \sum_{\substack{n=1 \\ m=n+1}}^{N-1} J_{n,m} |n\rangle\langle m| \qquad \text{(SI-6)}$$

where E_n is the transition energy of the n^{th} monomer and |n> is the state in which it is excited. $J_{n,m}$ is the intermolecular resonance interaction between the n^{th} and the m^{th} monomers ($J_{n,n+1}$=J) and N is the total number of monomers in the aggregate chain. The disorder is introduced as fluctuations of the monomer transition energies (diagonal disorder) or of the intermolecular interactions (off-diagonal disorder). The purpose of modeling the exciton structure is not to obtain any quantitative information of the exciton states, but rather show the relative energy differences of the states. Therefore, as a first approximation, we assume that the experimental

bathochromic shift (the energy difference the monomer absorption maximum to the J-aggregate absorption maximum) is equal to 2 J.

We used MatLab® to diagonalize the Hamiltonian for N = 250 monomers. J was chosen as -975 cm^{-1} according to the -1950 cm^{-1} bathochromic shift seen in Figure SI-1 (from 17575 cm^{-1}/ 569 nm to 15625 cm^{-1}/ 640 nm, which is in good agreement with previous measurements of the same molecule[6]). All energy parameters are measured in units of J here forth.

The Frenkel Hamiltonian describes the exciton states and absorption properties of a J-aggregate. Modeling of fluorescence is much more complex and goes beyond this Hamiltonian. At first approximation we assume thermal relaxation of the excitons within the exciton band. Even such simple picture gets complicated since not all states are equally accessible for a particular exciton because each state has its own location on the chain.[7] However, at first approximation we assume that emission maximum corresponds to the states located in the vicinity of the red edge of the exciton band (kT<<exciton band width).

As will be seen from the simulations below, this edge is situated at approximately -2.7 J. This energy then corresponds to the 'blue' fluorescence band of the aggregate #78. The 'red' band is shifted by 750 cm^{-1} which is 0.76 J. So, we should look for a single state by 0.8 J from all other low states forming the band edge.

Molecular disorder: Gaussian vs Lévy distributions

In the modeling we used either a Gaussian distribution or a heavy-tailed Lévy distribution with α=1.5, s=0.5 for the diagonal disorder. The Gaussian distribution had a standard deviation of σ=0.6 J, the Lévy distribution had FWHM=1.3 J (Figure SI-8a).

For each distribution, 100 realizations were made in order to calculate the absorption spectrum (Figure SI-8e and f shows the histogram with black face color generated by binning the oscillator strengths of all states, bin-size ≈ 0.01 J). Both distributions give the absorption bandwidth similar to that observed experimentally (~1000 cm^{-1}). Density of states (DOS) is also shown (c,d).

In order to see the exciton states for a single aggregate we look at the exciton states obtained from a single realization of the disorder.

In the case of the Gaussian disorder, we do not see any isolated state significantly below the group of several states that form the exciton band edge ((e), the amplitude of each red 'stick' gives the oscillator strength). Actually, even 100 realizations did not yield a drastically red-shifted state. The situation is different for the Lévy disorder. A state shifted from the edge by ≈0.8 J (Lévy state) is observed already in a single realization.

The dotted vertical lines in (a) show the standard deviations of the Gaussian distribution. In (b) the distributions are plotted in a logarithmic scale where the difference between the tails becomes obvious. It is clear that an 'outlier' monomer has orders of magnitude smaller chance to occur for the Gaussian disorder in comparison to the Lévy disorder. The vertical dotted line in (b) shows

the energy of the monomer which lead to formation of the Lévy state in the realization shown in (f).

We stress that the goal of these simulations is not to exactly fit the experimental data (a much more advanced model is needed for that), but to demonstrate the crucial difference between Gaussian and heavy-tailed Lévy distributions in regard to the formation of exciton outliers with a shift on the order of J in a single disorder realization.

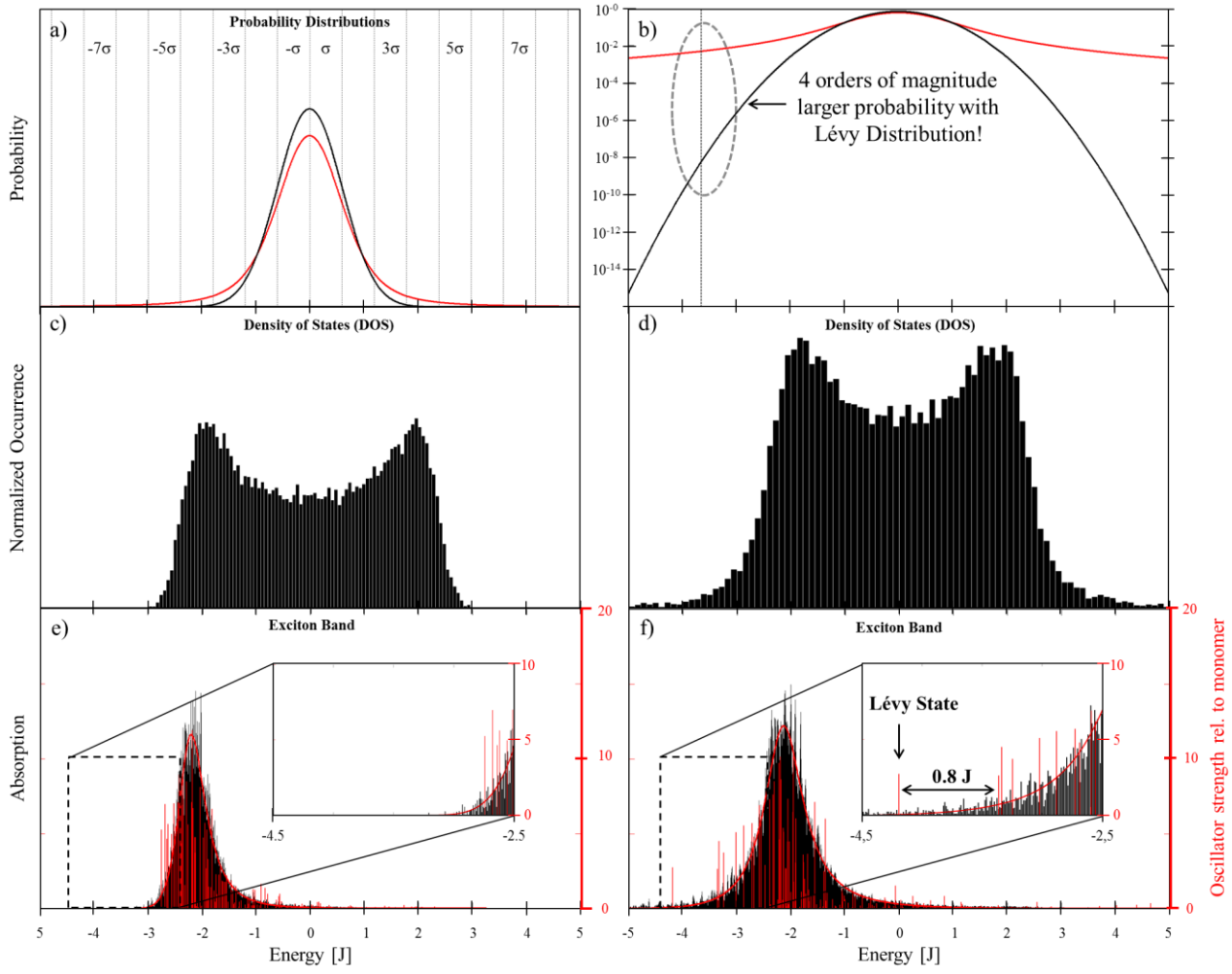

Figure SI-8 | Simulation results using different disorder distributions

(a) shows the different distributions used for the simulations (Gaussian – black, Lévy – red). (b) shows a logarithmic plot of the distributions to emphasize the differences in the tails. Vertical dotted line represents the outlier monomer forming the outlier exciton state in (f). (c-d) show the density of states (DOS) of the Gaussian and Lévy distributions respectively. (e-f) show the corresponding absorption spectra (black, 100 realization of the disorder) generated using the Gaussian and Lévy distributions respectively. The results from a single realization is plotted in red, where the oscillator strength is on the right y-axes.

SI- VII Experimental Setup

Figure SI-9 shows a schematic of the experimental setup used for the fluorescence measurements.The objective lens together with the additional imaging lens provided a magnification of 80X resulting in an effective pixel size of 200x200 nm. The diffraction grating had 150 grooves/mm and allowed for simultaneous observation of the three domains (spectral, intensity, spatial) as seen in the figure. The figure shows an example of experimental data of a single aggregate fluorescence in one acquisition frame where the emission pattern is seen in the zero order together with its spectrum in the first order diffraction. Depending on the sample under investigation, different excitation sources were used. For low temperature measurements, the sample was placed inside a cryostat as the figure shows.

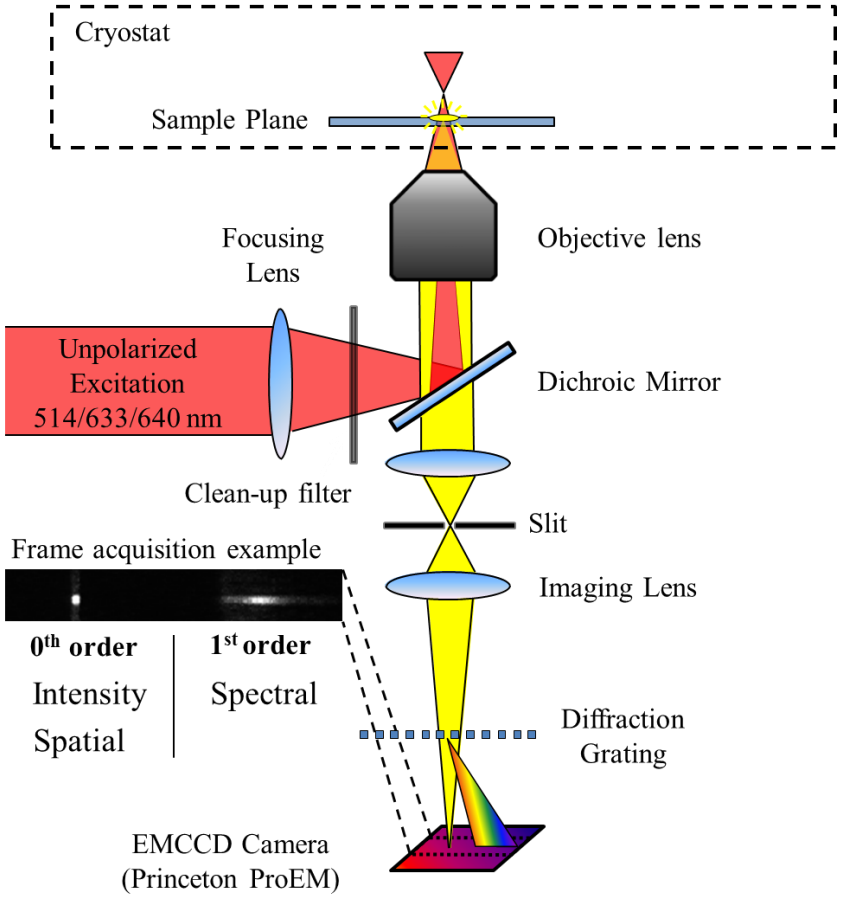

Figure SI-9 | Experimental Setup

References

1. Golub, G. & Reinsch, C. Singular value decomposition and least squares solutions. *Numer. Math.***14,** 403–420 (1970).

2. Johnson, S. Hierarchical clustering schemes. *Psychometrika***32,** 241–254 (1967).

3. Kojima, Isao; Kurahashi, M. Application of asymmetrical Gaussian/Lorentzian mixed function for x-ray photoelectron curve synthesis. *J. Electron Spectros. Relat. Phenomena***42,** 177–181 (1987).

4. Mirzov, O. *et al.* Polarization portraits of single multichromophoric systems: visualizing conformation and energy transfer. *Small***5,** 1877–1888 (2009).

5. Bednarz, M., Malyshev, V. & Knoester, J. Temperature dependent fluorescence in disordered frenkel chains: interplay of equilibration and local band-edge level structure. *Phys. Rev. Lett.***91,** 217401 (2003).

6. Kaiser, T. E., Stepanenko, V. & Würthner, F. Fluorescent J-aggregates of core-substituted perylene bisimides: studies on structure-property relationship, nucleation-elongation mechanism, and sergeants-and-soldiers principle. *J. Am. Chem. Soc.***131,** 6719–6732 (2009).

7. Scheblykin, I. G., Sliusarenko, O. Y., Lepnev, L. S., Vitukhnovsky, A. G. & Van der Auweraer, M. Excitons in Molecular Aggregates of 3, 3’-Bis-5, 5'-dichloro-9-ethylthiacarbocyanine (THIATS): Temperature Dependent Properties. *J. Phys. Chem. B***105,** 4636–4646 (2001).